


## Article

# Modelling above Ground Biomass in Tanzanian Miombo Woodlands Using TanDEM-X WorldDEM and Field Data

Stefano Puliti <sup>1,\*</sup>, Svein Solberg <sup>1</sup> , Erik Næsset <sup>2</sup>, Terje Gobakken <sup>2</sup>, Eliakimu Zahabu <sup>3</sup>, Ernest Mauya <sup>4</sup> and Rogers Ernest Malimbwi <sup>3</sup>

<sup>1</sup> Department of National Forest Inventory, Norwegian Institute for Bioeconomy Research (NIBIO), Ås 1430, Norway; svein.solberg@nibio.no

<sup>2</sup> Faculty of Environmental Sciences and Resource Management, Norwegian University of Life Sciences (NMBU), Ås 1430, Norway; erik.naesset@nmbu.no (E.N.); terje.gobakken@nmbu.no (T.G.)

<sup>3</sup> Department of Forest Mensuration and Management, Sokoine University of Agriculture (SUA), Morogoro 3000, Tanzania; zahabu@suanet.ac.tz (E.Z.); remalimbwi@yahoo.com (R.E.M.)

<sup>4</sup> Department of Forest Engineering and Wood Sciences, Sokoine University of Agriculture (SUA), Morogoro 3000, Tanzania; ernestmauya@gmail.com

\* Correspondence: stefano.puliti@nibio.no; Tel.: +47-936-78-891

Received: 11 August 2017; Accepted: 19 September 2017; Published: 22 September 2017

**Abstract:** The use of Interferometric Synthetic Aperture Radar (InSAR) data has great potential for monitoring large scale forest above ground biomass (AGB) in the tropics due to the increased ability to retrieve 3D information even under cloud cover. To date; results in tropical forests have been inconsistent and further knowledge on the accuracy of models linking AGB and InSAR height data is crucial for the development of large scale forest monitoring programs. This study provides an example of the use of TanDEM-X WorldDEM data to model AGB in Tanzanian woodlands. The primary objective was to assess the accuracy of a model linking AGB with InSAR height from WorldDEM after the subtraction of ground heights. The secondary objective was to assess the possibility of obtaining InSAR height for field plots when the terrain heights were derived from global navigation satellite systems (GNSS); i.e., as an alternative to using airborne laser scanning (ALS). The results revealed that the AGB model using InSAR height had a predictive accuracy of  $RMSE = 24.1 \text{ t} \cdot \text{ha}^{-1}$ ; or 38.8% of the mean AGB when terrain heights were derived from ALS. The results were similar when using terrain heights from GNSS. The accuracy of the predicted AGB was improved when compared to a previous study using TanDEM-X for a sub-area of the area of interest and was of similar magnitude to what was achieved in the same sub-area using ALS data. Overall; this study sheds new light on the opportunities that arise from the use of InSAR data for large scale AGB modelling in tropical woodlands.

**Keywords:** InSAR; TanDEM-X; above ground biomass; tropical woodlands; LiDAR; forest monitoring; REDD+

## 1. Introduction

Forests play a critical role in the global carbon budget with deforestation accounting for 10% of the anthropogenic carbon emissions, as estimated in the fifth assessment report of the Intergovernmental Panel on Climate Change (IPCC) [1]. As a result, the United Nations Framework Convention on Climate Change (UNFCCC) established a program aimed at reducing emissions from deforestation and land degradation in tropical countries (i.e., REDD+ program) [2]. In order to ensure a successful implementation of REDD+, the UNFCCC has proposed a system based on financial compensations for reducing emissions. A critical aspect in this system lies in the development of robust methods

for measuring, reporting and verifying carbon stock changes [3]. In order to become operational, these methods in addition to being robust and precise should also be cost-efficient. Thus, in the past decade, great effort has been dedicated to better understanding the possibility of using remotely sensed data for monitoring changes in forest carbon and above ground biomass (AGB) in tropical countries [4]. Of the variety of data sources, 3D remotely sensed data are increasingly being used due to their ability to describe the vertical structure of the forest canopy and the high correlation between AGB and canopy height. Within the different 3D remotely sensed data available nowadays, Interferometric Synthetic Aperture Radar (InSAR) data have the advantage of providing large area coverage even under cloud cover, hence their use in tropical countries for monitoring changes in forest resources. One approach to using InSAR for forest monitoring is through complex correlation, i.e., the coherence magnitude for a pair of SAR acquisitions. Relationships between coherence and forest height or biomass have been demonstrated with repeat-pass L-band acquisitions with PALSAR [5] and single-pass X-band acquisitions with TanDEM-X [6,7]. An advantage of this approach is that a digital terrain model (DTM) is not required, however, the performance depends on the season and saturation effects may occur. Another approach not requiring a DTM is to acquire dual-band InSAR data, i.e., combining a short and a long wavelength, where the long-wavelength digital elevation model (DEM) will represent the terrain elevation [8]. However, this approach is not feasible for large scale monitoring. In the case where a high quality DTM is available it has been demonstrated that forest height and biomass can be estimated either based on the height of the phase centre above the ground [9] or based on a more sophisticated approach utilizing the ground-corrected complex coherence [10]. Although the height of the phase centre in a tropical forest appears to be fairly stable between acquisitions [11], weather conditions, phenology [12–14], terrain steepness and ascending or descending mode acquisitions can cause differences in height [15]. One particular approach to overcome these limitations is to monitor height changes rather than heights, which would not require a DTM, and to combine several acquisitions. The use of DEMs such as the WorldDEM may be particularly suitable as it is based on repeated acquisitions.

Within the REDD+ context the main interest lies in the estimation and mapping of AGB changes over time as this allows for the quantification of the reduction in emissions and corresponding financial compensations. Solberg et al. [16,17] proposed a methodology using multi-source InSAR data to monitor changes in forest AGB, possibly providing inputs to the global carbon budget and REDD+. One of the major advantages of this method is that it does not require any spatially continuous terrain information (i.e., a digital terrain model). This is because the AGB change is derived by applying a proportional relationship between AGB and InSAR height together with height changes between two InSAR digital elevation models (DEMs). As a first step, the relationship between InSAR height above ground ( $H$ ) and AGB is estimated for a sample of field inventory plots at one point in time using a regression model through the origin (i.e.,  $\beta_0 = 0$ ).

$$AGB = \beta_1 H + e \quad (1)$$

The parameter estimate  $\beta_1$  is then used as the proportionality factor for estimation of AGB change ( $\Delta AGB$ ) and the corresponding emission ( $E$ ) given height change ( $\Delta H$ ) per meter as an alternative to the widely used fixed emission factors per area unit given an area ( $A$ ) according to the equation:

$$E = A \times \Delta H \times \beta_1 \quad (2)$$

This approach requires that the model is valid at both points in time as reported by Solberg et al. [16] who proved that InSAR data produced reasonably accurate  $\Delta AGB$  predictions in boreal forest using InSAR DEMs from the Shuttle Radar Topography Mission (SRTM) and a DEM from TanDEM-X with a root mean square error (RMSE) value of  $55 \text{ t} \cdot \text{ha}^{-1}$  (43% of the mean AGB). However, careful processing is required when using SRTM DEMs, which have biases of several meters varying at the continental scale [18] as well as artifacts in the form of stripes [19]. Studies in tropical forests

have yielded variable results. Neeff et al. [20] obtained a similar relationship for a virgin rainforest in Brazil. Gama et al. [21] obtained a curvilinear relationship, while for African tropical forests Solberg et al. [15,17] obtained noisier results having  $RMSE$  values of  $40 \text{ t} \cdot \text{ha}^{-1}$  (78% of the mean  $AGB$ ) and  $203 \text{ t} \cdot \text{ha}^{-1}$  (44% of the mean  $AGB$ ) in Tanzanian miombo woodlands and dense tropical forests, respectively. The latter cases suffered from small and few field inventory plots, not taking into account the large size of single trees in those forests, thus the applicability of models like Equation (1) remains uncertain. Moreover, the potential accuracy of InSAR depends on the quality of the algorithms used for InSAR processing and DEM mosaicking, and it is likely that the WorldDEM is a more consistent and seamless DEM than the single TanDEM-X acquisitions used in previous research studies. Further studies in tropical forests are required in order to improve the understanding and accuracy of the relationship between high quality InSAR height data and  $AGB$  in tropical forests.

Accurate terrain information (i.e., ground heights) is required for the sample of field inventory plots used for the estimation of the parameter  $\beta_1$ . Airborne laser scanning (ALS) is an excellent source of ground heights, however these data are rarely available in tropical areas. Hence, it would be greatly beneficial if the ground height of the field plots could be recorded in the field using global navigation satellite systems (GNSS).

### Objectives

The primary objective of this study was to describe the relationship between  $AGB$  and InSAR height in a tropical miombo woodland. Specifically, the aim was to use improved data compared to Solberg et al. [17] by using more accurate InSAR height data, i.e., the WorldDEM, and by applying a larger field inventory data set. A secondary objective was to determine the possibility to establish this relationship without the need of any ALS terrain information, hence increasing the area of application of the developed methods.

## 2. Materials and Methods

### 2.1. Study Area

The area of interest (AOI) was located in Liwale District ( $9^{\circ}52' - 9^{\circ}58'S$ ,  $38^{\circ}19' - 38^{\circ}36'E$ ) and covers a total of  $15,867 \text{ km}^2$ . The area is characterized by a mosaic of agricultural areas and miombo woodlands. The miombo woodlands in the AOI are composed of several forest types, ranging from dry to wet sub-types. A rich species composition characterizes the AOI including species related to *Brachystegia* sp., *Julbernardia* sp. and *Pterocarpus angolensis*.

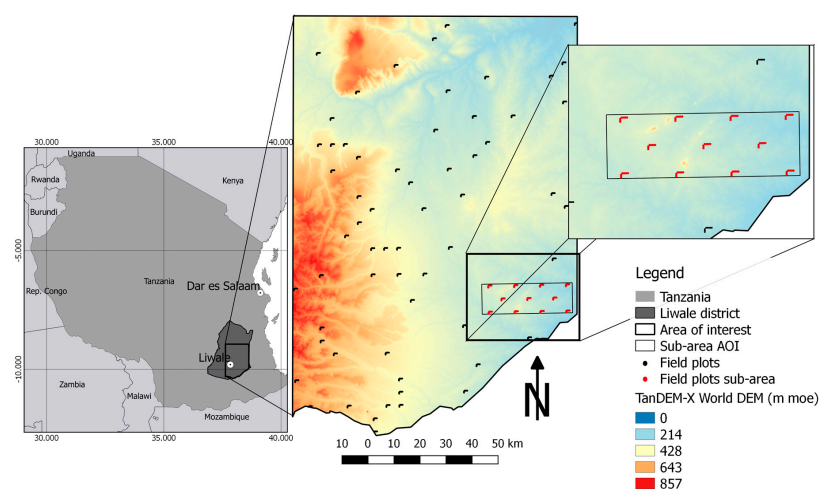


**Figure 1.** Overview of the area of interest and sampling design. The sub-area of the area of interest was used to compare with previous studies.

The area has been part of previous research thus further description of the study area can be found in Mauya et al. [22] and Ene et al. [23,24]. An overview of the AOI is provided in Figure 1.

## 2.2. Field Data

A total of 513 field plots were available for this study. These were grouped in 65 clusters with 8 field plots each forming an L-shape (see Figure 2). These represented a subset of the field plots acquired within the national forestry resource monitoring and assessment of Tanzania (NAFORMA) program [25]. The NAFORMA program represents the first effort to harmonize and update forest inventory in Tanzania. Its objective is to produce information to support national and international policy processes in regard to sustainable forest management (SFM), the reduction of emissions from deforestation and forest degradation (REDD+), and greenhouse gas (GHG) emissions. The NAFORMA inventory adopts a two-phase stratified systematic cluster design with double sampling for stratification [26]. In the first phase, L-shaped clusters were selected according to a grid of 5 km  $\times$  5 km and assigned to a stratification based on: (1) plots' accessibility; (2) predicted forest growing stock; and (3) slope. Furthermore, in the second phase the stratum-specific sampling intensities were defined using optimal allocation [27]. The distance between consecutive plots within a cluster was 250 m. Further details on the sampling design can be found in Tomppo et al. [26,28]. In this study the field dataset used by Solberg et al. [17] and by Næsset et al. [29] increased nearly five times, thus providing the possibility to better understand the effect of the increased sample size on the AGB models.

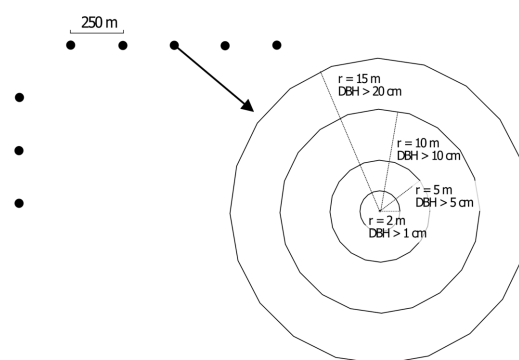


**Figure 2.** Overview of the the national forestry resource monitoring and assessment of Tanzania NAFORMA cluster with detail on a single field plot. According to the NAFORMA field plot design the trees' diameters at breast height (DBH) for all trees with DBH >1, 5, 10 and 20 cm were recorded on concentric plots with radii of 2, 5, 10 and 15 m, respectively.

Field plot measurements were carried out in February–June 2012 and included the measurements in concentric circles with diameters of 2, 5, 10 and 15 m from trees with diameter at breast height (DBH) of >1, 5, 10 and 20 cm, respectively. DBH measurements were performed for each tree according to the abovementioned concentric thresholds while tree height was measured for every fifth tree. For those trees that did not include height measurement, tree height was predicted using diameter-height models fitted using the height sample trees. A tree was measured if it was taller than or equal to 1.35 m and, according to the Food and Agriculture Organization Global Forest Resources Assessment (FAO FRA) definitions [30], if it was capable of reaching 5 m in height in situ. Cactuses, palms, bamboos and shrubs were not recorded as trees. The choice of the concentric plots was driven by the need to increase the accuracy of the measurement and sampling intensity of large trees, while also saving time. The radii of the concentric circles and respective thresholds for DHB measurements were defined subjectively according to local knowledge and practical reasons [26]. Overall, measured tree heights were on average 9.3 m and ranged from 1 to 41 m, while the DBH was 17.4 cm on average and ranged between 1 cm and 210 cm. Above ground biomass was then obtained using DBH and



height as input in the allometric models by Mugasha et al. [31] developed for miombo woodlands in Tanzania. Summary statistics (i.e., mean, range and standard deviation) for AGB are reported in Table 1. Additional differential dual-frequency global positioning system and global navigation satellite systems (DGNSS) measurements were acquired in 2014 and for most of the plots ( $n = 500$ ) sub-meter accuracy measurements were performed using a DGNSS antenna mounted on a 2.9 m pole located in the plot center. Field plots where DGNSS measurements were not available ( $n = 13$ ) were discarded from further analysis as DGNSS measurements were required for the purpose of this study. As reported by Ene et al. [24], the estimated precision of the planimetric coordinates was 0.132 m on average.

**Table 1.** Summary statistics for above ground biomass (AGB;  $\text{t}\cdot\text{ha}^{-1}$ ) for the AOI and the sub-area of the AOI.

	Number of Observations	Mean	Range	Standard Deviation
AOI	500	61.1	0–350.3	48.6
Sub-area AOI	88	51.3	0–213.4	45.9

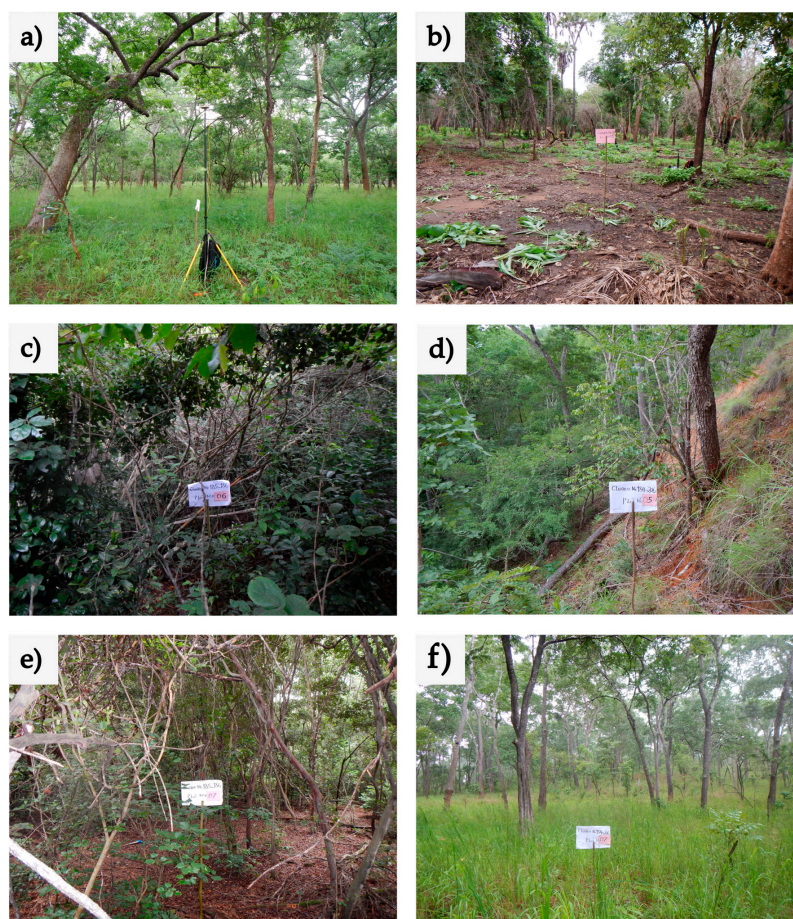


**Figure 3.** Overview of the field measurements and forest types for some of the measured field plots. In particular the photos illustrate: (a) field plot center with equipment used for dual-frequency global positioning system and global navigation satellite systems (DGNSS) measurements; (b) agroforestry system including some palms; (c) field plot with large tree density; (d) field plot on a slope and with large above ground biomass (AGB) values; (e) field plot with medium tree density; (f) field plot with open canopy cover.

To provide a thorough comparison between the results of the present study against previous research by Solberg et al. [17] and Næsset et al. [29], we used the 88 field plots from those studies

located in a sub-area of the present AOI. Half of these were a subset of the total number of plots (i.e., the 513 plots previously described), while the other half were part of a new set of plots acquired by doubling the clusters' sampling intensity (see Figure 1). The field data for the sub-area were acquired two years after (i.e., 2014) the acquisition of the field data used for the entire AOI (i.e., 2012). A further description of this additional field plot dataset can be found in Næsset et al. [29]. Table 1 summarizes AGB for the entire AOI and for the sub-area of the AOI, while Figure 1 illustrates the sampling design in the entire AOI and in the sub-area used for further validation. In Figure 3, the pictures taken during the field campaign illustrate different forest structures included in the field measurements.

### 2.3. TanDEM-X WorldDEM

The WorldDEM is a global DEM available as a commercial product [32] in various spatial resolutions; the 30 m  $\times$  30 m resolution version was used in this study. The DEM is based on repeated acquisitions with various across-track baselines from the TanDEM-X mission. TanDEM-X is a mission with two satellites moving in formation and acquiring single-pass X-band SAR data for interferometric applications, in particular DEM processing [33].

### 2.4. ALS Data

Leaf-on ALS data were acquired in February–March 2012 using a Leica ALS-70 sensor. The average pulse density over the entire area was 1.9 pulses  $\text{m}^{-2}$ . The ALS data acquisition obtained partial coverage of the entire AOI by means of 32 parallel strips (i.e., in the east–west direction). These strips covered the entire set of field plots. A further description of the ALS data can be found in Ene et al. [23]. In this study ALS data was used exclusively for extraction of ground elevation information, thus all points classified as non-ground were discarded from any further analysis.

### 2.5. Normalization of TanDEM-X Height

Prior to fitting a model linking AGB and TanDEM-X height, the latter was normalized, i.e., converted from heights above the ellipsoid to heights above the ground ( $\Delta z$ ), or by subtracting the ground height from the TanDEM-X height. The TanDEM-X height value for each plot was extracted as the pixel value coinciding with the plot center. The possibility of replacing ALS data as a source of ground height information with DGNSS measurements was assessed by comparing the AGB model fitted with TanDEM-X data normalized using ALS ground height ( $\Delta z_{\text{ALS}}$ ) to an alternative model using TanDEM-X data normalized with DGNSS ( $\Delta z_{\text{DGNSS}}$ ). The high Pearson's correlation coefficient between the DGNSS height and ALS height ( $r = 0.99997$ ) justified the use of the former as an alternative to ALS (see Figure 4). Even though there was a high correlation between the DGNSS and ALS ground heights, the differences between the two values ranged between  $-4.3$  m and  $5.6$  m (Figure 4). Such differences may be partly attributable to differences in the measurement of DGNSS and ALS ground height values, where the former were obtained by single measurement of the plot center and the latter by averaging plot level ground values. However, because of the lack of additional higher precision measurements of the ground height, it was not possible to determine which dataset was more precise.

### 2.6. Model Fitting

Two simple linear regression models though the origin were fitted using either  $\Delta z_{\text{ALS}}$  or  $\Delta z_{\text{DGNSS}}$  and the field measured AGB. Previous studies by Solberg et al. [16,17] demonstrated that the adoption of a no-intercept model compared to an intercept model has little effect on the performance of the model and is biologically reasonable by predicting zero biomass for zero InSAR height. Furthermore, by setting  $\beta_0 = 0$  the  $\beta_1$  parameter can be directly interpreted as the emission factor, hence it simplifies further use of the relationship between InSAR height and AGB.

The models' predictive accuracy was assessed by performing a leave-one-cluster-out cross validation (LOCOCV), according to which each cluster was removed iteratively and the observations

within the cluster used as validation. The root mean square error ( $RMSE$ ,  $t \cdot ha^{-1}$ ) and  $RMSE$  as percentage of the mean field  $AGB$  ( $RMSE\%$ ) were calculated and adopted as a measure of the accuracy of the predictions. Given a sample of  $n$  field plots the  $RMSE$  was calculated as:

$$RMSE = \sqrt{\frac{\sum_{i=1}^n (y_i - \hat{y}_i)^2}{n}} \quad (3)$$

Further assessment of the models' performance included the visual inspection of the residuals. Lastly, the study adopted the same methodology to the sub-area of the AOI where 88 field plots were available. Because of the lack of a large sample in this case, a leave-one-plot-out cross validation was conducted to obtain  $RMSE$  and  $RMSE\%$ .

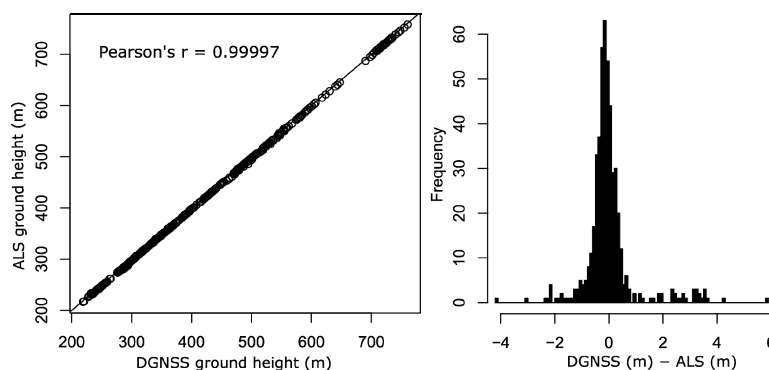


**Figure 4.** Relationship between DGNSS ground height measured in the field against ALS derived ground height. The scatterplot on the left shows the relationship between the two height measures including the Pearson's correlation coefficient. The line in the scatterplot represents the 1:1 line. The histogram on the right shows the distribution of the differences between DGNSS height and airborne laser scanning (ALS).

### 3. Results

The results revealed that both models (i.e., using either  $\Delta z_{ALS}$  or  $\Delta z_{DGNSS}$ ) performed very similarly. The model based on  $\Delta z_{DGNSS}$  resulted in the estimation of a slightly smaller  $\beta_1$  (11.7) than the alternative one fitted using  $\Delta z_{ALS}$  (12.1). Given the overlap in the confidence intervals (see Figure 5) and according to a two-sided t-test this difference was not significant ( $p$ -value < 0.05).

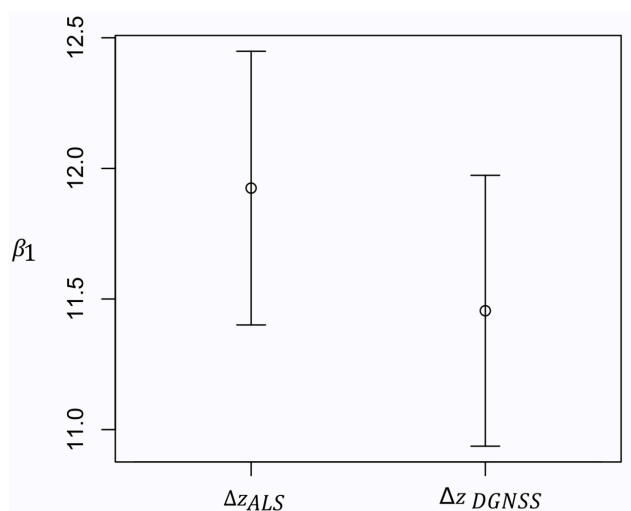


**Figure 5.** Parameter estimates for  $\beta_1$  with 95% confidence intervals for the  $\Delta z_{ALS}$  and  $\Delta z_{DGNSS}$  model.

The predictive accuracy of the cross validated models was similar between  $\Delta z_{ALS}$  and  $\Delta z_{DGNSS}$  models (see Figure 6), with  $RMSE$  and  $RMSE\%$  values equal to  $24.1 \text{ t}\cdot\text{ha}^{-1}$  (38.8%) and  $24.8 \text{ t}\cdot\text{ha}^{-1}$  (39.9%) for the models using  $\Delta z_{ALS}$  and  $\Delta z_{DGNSS}$ , respectively.

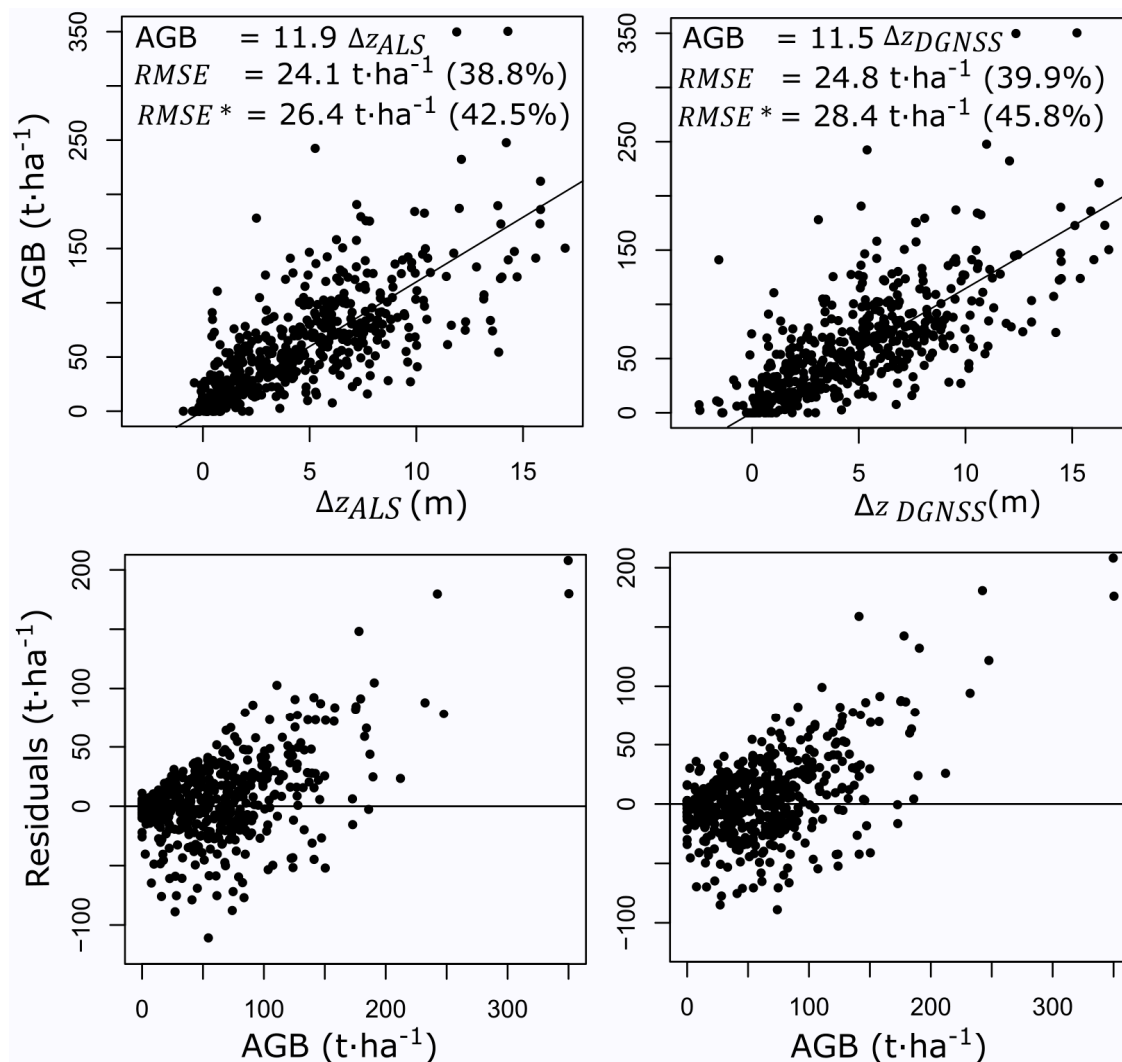


**Figure 6.** Scatterplot of heights (m) from  $\Delta z_{ALS}$  (left) and  $\Delta z_{DGNSS}$  (right) against AGB ( $\text{t}\cdot\text{ha}^{-1}$ ). The model parameter  $\beta_1$  estimate,  $RMSE$  and  $RMSE\%$  (in parenthesis) are reported for both models. The  $RMSE^*$  reports the results of the leave-one-cluster-out cross validation. The plots in the lower row represent the models' residuals plotted against field plot AGB ( $\text{t}\cdot\text{ha}^{-1}$ ) for  $\Delta z_{ALS}$  (left) and  $\Delta z_{DGNSS}$  (right).

The visual analysis of the scatterplot of the residuals (Figure 6) revealed the presence of heteroscedasticity for both  $\Delta z_{ALS}$  and  $\Delta z_{DGNSS}$  models. Furthermore, effects of saturation were detectable for plots with AGB larger than approximately  $186 \text{ t}\cdot\text{ha}^{-1}$ , i.e., all the plots with AGB larger than approximately  $186 \text{ t}\cdot\text{ha}^{-1}$  were under-predicted.

The results of the comparison of the  $\Delta z_{ALS}$  AGB model fitted using only the plots located in the sub-area of the AOI are reported in Table 2. These revealed that the  $\Delta z_{ALS}$  model presented in the current study had a predictive accuracy of similar magnitude to a model where seven predictor variables from ALS data were used. The comparison with the study by Solberg et al. [17] revealed that the use of TanDEM-X WorldDEM at medium resolution (i.e.,  $30 \text{ m} \times 30 \text{ m}$  pixels) resulted in a smaller  $\beta_1$  estimate (11.0) and in a decrease in  $RMSE$  compared to higher resolution TanDEM-X data



(i.e., 10 m  $\times$  10 m pixels). Furthermore, compared to the other remotely sensed data sources compared by Næsset et al. [29], the use of TanDEM-X WorldDEM always led to a reduction in the *RMSE*.

**Table 2.** Comparison of the results for  $\Delta z_{ALS}$  AGB model fitted in the current study against previous ones conducted in the sub-area of the AOI using alternative auxiliary data. The comparison included the number of predictor variables and the predictive accuracy using leave-one-plot-out cross validation (i.e., *RMSE* and *RMSE*<sub>%</sub> ).

Study	Auxiliary Data	<i>n.</i> Predictor Variables	$\beta_1$	<i>RMSE</i> * (t·ha <sup>−1</sup> )	<i>RMSE</i> *% (%)
Current study	TanDEM-X WorldDEM™	1	1.0	30.4	59.2
Næsset et al. 2016	ALS	7	-	31.8	62.0
Næsset et al. 2016	RapidEye	4	-	34.2	66.6
Solberg et al. 2015	TanDEM-X	1	14.1	41.3	80.5
Næsset et al. 2016	Global Landsat maps	1	-	44.6	86.9
Næsset et al. 2016	Global PALSAR maps	2	-	46.6	90.7

*RMSE*\* and *RMSE*\*% = *RMSE* and *RMSE*<sub>%</sub> values obtained using a leave-one-plot-out cross validation.

#### 4. Discussion

This study aimed at assessing the possibility of using InSAR data from TanDEM-X DEM to model AGB in tropical woodlands. The biggest contribution of this study is that it provided new and complementary knowledge to an AOI which had been the object of extensive research efforts in the past five years. In addition to the large field data, several remotely sensed data including ALS, RapidEye, Landsat 8 and global forest maps were acquired as part of this effort. As a result, previous studies conducted in the same area provided us with a unique opportunity to compare our results using alternative remotely sensed auxiliary data.

Overall, the current study reported unique figures in terms of the predictive accuracy of the models. The *RMSE* and *RMSE*<sub>%</sub> values found were smaller (*RMSE* = 24.1–24.8 t·ha<sup>−1</sup>; *RMSE*<sub>%</sub> = 38.8–39.9%) than a previous study by Solberg et al. [17] where TanDEM-X normalized data (i.e.,  $\Delta z_{ALS}$ ) was used to model AGB in the same AOI but using a subset of 88 field plots (*RMSE* = 40 t·ha<sup>−1</sup>; *RMSE*<sub>%</sub> = 78.0%). The improved accuracy obtained in the present study is likely a result of the use of combined and repeated TanDEM-X acquisitions with both small and large across-track baselines in the WorldDEM, whereby random errors and phase unwrapping problems are reduced. Furthermore, it is likely that the software developed by German Aerospace Center (DLR) for the production of the WorldDEM allows obtaining more accurate data than that which is achievable for researchers using commercial software (e.g., SARscape) thanks to enhanced block-adjustment and seamless mosaicking of single acquisitions. The accuracy of the parameter estimate is also improved (i.e., reduced standard error of the estimated  $\beta_1$  parameter) in the present study in comparison with that of Solberg et al. [17] because the sample size was increased by approximately 5.7 times. The lower spatial resolution of the present TanDEM-X data might have had a minor influence on the accuracy, although this could be further studied by redoing the present study with the WorldDEM at 12 m resolution. Furthermore, the results of the current study were also directly comparable with the results by Ene et al. [23] who fitted a linear mixed-effects model using the same AGB observations used in this study but using ALS variables as predictors. It was encouraging to see that the *RMSE* values found in this study were smaller than in Ene et al. [23] who reported a *RMSE* of 31.16 t·ha<sup>−1</sup> (47.4% of the mean AGB). The validity of this comparison is also confirmed by the findings by Næsset et al. [29] who, in the sub-area of our AOI, found larger cross-validated *RMSE* than the model presented in this study both for ALS (31.8 t·ha<sup>−1</sup>; 62.0%) and RapidEye data (34.2 t·ha<sup>−1</sup>; 66.6%). Despite the consistency of these findings across the entire AOI and in the sub-area of the AOI, it was somewhat surprising to see that medium-resolution TanDEM-X WorldDEM data could yield smaller *RMSE* and *RMSE*<sub>%</sub> (30.4 t·ha<sup>−1</sup>; 59.2%) than ALS data. Generally, the use of remotely sensed data at a resolution coarser than the field observations (e.g., TanDEM-X WorldDEM) can result in the spatial mismatch between the remotely sensed signal and the field observation because of a different geographical location and extent of the

two measures. Such a mismatch often results in a degradation of the correlation between remotely sensed data and field plots, especially when there are large variations in forest structures. In this study it is possible that the *AGB* model based on TanDEM-X WorldDEM did not suffer to a great extent from such an effect because the canopy height in the miombo woodlands is rather uniform. It is possible that the lower resolution of the TanDEM-X WorldDEM data was a minor issue compared to other problems that affected the comparison with the results of ALS models by Næsset et al. [29].

As described by Næsset et al. [29] one of the main sources of uncertainty in their ALS models may have been derived from the use of concentric field plots. If on one hand the use of concentric plots can be efficient, on the other hand it may be unsuitable when using ALS data. In the study by Næsset et al. [29], ALS data were extracted for plots of fixed radius (i.e., 15 m) while *AGB* was measured using variable radii. In this regard, Næsset et al. [29] noted that for some plots small trees were found in the outer part of the plots (thus were not measured in the field) while no or few small trees were present in the the plot center. In these specific cases, the ALS point cloud included pulses from those small trees on the outer edge while the corresponding biomass was not measured in the field. It is likely that such an issue may have introduced undesired noise in the relationship between ALS variables and *AGB*, thus degrading the quality of the model's predictions. This effect could have been further aggravated by the fact that certain species (for example cactuses, palms, bamboos and shrubs) were not measured but may have accounted for part of the ALS returns. Such noise due to small trees in the outer part of the field plot and other species present in the dominated canopy layer was possibly alleviated when using InSAR data as these data mainly describe the top of the canopy (i.e., dominant layer). It is therefore evident that further studies adopting fixed-radius plots are needed for a fair evaluation of TanDEM-X WorldDEM against ALS data.

Despite the need of confirming these results in other forest types and with more suitable sampling designs, the findings of this study suggest that TanDEM-X WorldDEM data can indeed provide valuable *AGB* explanatory variables. The comparison with alternative space-borne remotely sensed data indicated that *AGB* models using TanDEM-X WorldDEM data had a larger predictive accuracy than other models using either RapidEye, global Landsat maps [34], or global PALSAR maps [35] for which Næsset et al. [29] reported *RMSE* values of  $32.2 \text{ t} \cdot \text{ha}^{-1}$  (62.7%),  $43.6 \text{ t} \cdot \text{ha}^{-1}$  (85.0%) and  $45.3 \text{ t} \cdot \text{ha}^{-1}$  (88.3%), respectively. Consistent with studies conducted in similar forest types, the present one reported effects of saturation for field plots with *AGB*  $>186 \text{ t} \cdot \text{ha}^{-1}$ . This effect manifests itself as the under-prediction of large *AGB* values and is a common drawback when modelling forest volumetric properties using remotely sensed data especially in complex forest types. Furthermore, it is important to mention that despite the fact that saturation was observed, it was limited to 14 plots (2.8% of the sample size) hence its overall effect for large-scale *AGB* models might be negligible.

Concerning the  $\beta_1$  parameter estimate linking *AGB* with  $\Delta z_{ALS}$  or with  $\Delta z_{DGNSS}$  (i.e., proportionality factor or emission factor), the current study reported slightly smaller values (11.9–11.5) than what was previously found by Solberg et al. [17], which is attributable to a larger uncertainty in that study as a result of being based on fewer field plots. The  $\beta_1$  parameter estimate found in the sub-area object of study was 27% smaller than what was found by Solberg et al. [17], which may be due to the coarser resolution of the auxiliary data used in this study, which resulted in a reduction of local height variations. Despite the loss in height variations, the use of TanDEM-X WorldDEM data led to a smaller standard error for the  $\beta_1$  estimate ( $0.87 \text{ t} \cdot \text{ha}^{-1} \cdot \text{m}^{-1}$ ) compared to Solberg et al. [17] ( $1.08 \text{ t} \cdot \text{ha}^{-1} \cdot \text{m}^{-1}$ ). Thus, because of the larger precision of the estimate and the improvements in the processing of the TanDEM-X data, it is reasonable to believe that the  $\beta_1$  estimate reported in this study is more reliable than the estimate reported by Solberg et al. [17]. The difference of the estimated  $\beta_1$  value between  $\Delta z_{ALS}$  and  $\Delta z_{DGNSS}$  was  $0.4 \text{ t} \cdot \text{ha}^{-1} \cdot \text{m}^{-1}$ , however this difference was not significant.

One finding that was highlighted by this study is that DGNSS data collected in the field campaign can indeed provide reliable information on the ground elevation, thus enabling the normalization of TanDEM-X data. This opens the possibility to apply this methodology to areas where accurate digital terrain models from ALS are not available, which is often the case in tropical areas. Among the reasons

that hinder the acquisition of the availability of ALS data in tropical areas, some of the most prominent limitations relate to the landscapes (i.e., vast areas with lack of infrastructure), the weather conditions (i.e., cloud cover) and the logistics (i.e., lack of readily available technology). In order to obtain accurate DGNSS measurements, high-grade GNSS receivers and base stations are required, and this could prove to be challenging when conducting forest inventories in tropical countries. In addition, obtaining accurate GNSS positioning in tropical forests can be considerably more challenging than in this study, which was conducted in a predominantly open woodland area. Future research should therefore address the effect of positional errors, especially in regard to the z coordinate on the models linking AGB with  $\Delta z_{DGNSS}$ .

## 5. Conclusions

Despite the simplicity of the statistical analysis, this study sheds new light on the possibility of using 3D data from TanDEM-X WorldDEM data for modelling AGB in tropical forests. The findings from this study were some of the first in the literature suggesting that TanDEM-X WorldDEM data may provide similarly accurate AGB predictions to ALS data in tropical woodlands. These results are strongly encouraging for the future use of these data, however more research is needed to better understand the potential to use TanDEM-X WorldDEM data to model AGB in a variety of forest types. To answer this need, research efforts are underway to explore the potential of TanDEM-X WorldDEM data to model AGB in forest types including woodland forest in other regions, tropical rainforest and boreal forests. Furthermore, future research should address the possibility to apply the proportional relationship between AGB and InSAR height derived in this study to height differences between multi-temporal InSAR data in order to estimate AGB changes over time.

**Acknowledgments:** The field data used in this project was funded by the Royal Norwegian Embassy in Tanzania as part of the Norwegian International Climate and Forest Initiative as part of the project “Enhancing the measuring, reporting and verification (MRV) of forests in Tanzania through the application of advanced remote sensing techniques”. The German Aerospace Centre (DLR) is acknowledged for providing the WorldDEM data for this study through the supported science AO DEM\_FOREST1646.

**Author Contributions:** Stefano Puliti and Svein Solberg conceived and designed the experiments; Stefano Puliti performed the data analysis and wrote the paper; Svein Solberg, Erik Næsset and Terje Gobakken contributed with comments on the paper; Eliakimu Zahabu, Ernest Mauya and Roger Ernest Malimbwi acquired the field data.

**Conflicts of Interest:** The authors declare no conflict of interest.

## References

1. IPCC. Summary for policymakers. In *Climate Change 2013: The Physical Science Basis*; Contribution of Working Group I to the Fifth Assessment Report of the Intergovernmental Panel on Climate Change; Stocker, T.F., Qin, D., Plattner, G.-K., Tignor, M., Allen, S.K., Boschung, J., Nauels, A., Xia, Y., Bex, V., Eds.; IPCC: Geneva, Switzerland, 2013.
2. UNFCCC. *Unfccc 2011 Report of the Conference of the Parties on Its 16th Session, Held in Cancun from 29 November to 10 December 2010, Addendum: Part Two: Action Taken by the Conference Of the Parties at Its 16th Session*; Bonn: United Nations Framework Convention on Climate Change; UNFCCC: New York, NY, USA, 2011.
3. Herold, M.; Skutsch, M. Monitoring, reporting and verification for national redd plus programmes: Two proposals. *Environ. Res. Lett.* **2011**, *6*. [[CrossRef](#)]
4. Sanchez-Azofeifa, A.; Antonio Guzmán, J.; Campos, C.A.; Castro, S.; Garcia-Millan, V.; Nightingale, J.; Rankine, C. Twenty-first century remote sensing technologies are revolutionizing the study of tropical forests. *Biotropica* **2017**, *49*, 604–619. [[CrossRef](#)]
5. Thiel, C.J.; Thiel, C.; Schmulius, C.C. Operational large-area forest monitoring in siberia using alos palsar summer intensities and winter coherence. *IEEE Trans. Geosci. Remote Sens.* **2009**, *47*, 3993–4000. [[CrossRef](#)]
6. Treuhaft, R.; Goncalves, F.; dos Santos, J.R.; Keller, M.; Palace, M.; Madsen, S.N.; Sullivan, F.; Graca, P. Tropical-forest biomass estimation at X-band from the spaceborne tandem-x interferometer. *IEEE Geosci. Remote Sens. Lett.* **2015**, *12*, 239–243. [[CrossRef](#)]

7. Olesk, A.; Praks, J.; Antropov, O.; Zalite, K.; Arumäe, T.; Voormansik, K. Interferometric sar coherence models for characterization of hemiboreal forests using tandem-x data. *Remote Sens.* **2016**, *8*, 700. [[CrossRef](#)]
8. Rombach, M.; Moreira, J. Description and applications of the multipolarized dual band orbisar-1 insar sensor. In Proceedings of the International Radar Conference 2003, Adelaide, Australia, 3–5 September 2003.
9. Solberg, S.; Astrup, R.; Breidenbach, J.; Nilsen, B.; Weydahl, D. Monitoring spruce volume and biomass with insar data from tandem-x. *Remote Sens. Environ.* **2013**, *139*, 60–67. [[CrossRef](#)]
10. Soja, M.J.; Persson, H.J.; Ulander, L.M.H. Estimation of forest biomass from two-level model inversion of single-pass insar data. *IEEE Trans. Geosci. Remote Sens.* **2015**, *53*, 5083–5099. [[CrossRef](#)]
11. Solberg, S.; Lohne, T.-P.; Karyanto, O. Temporal stability of insar height in a tropical rainforest. *Remote Sens. Lett.* **2015**, *6*, 209–217. [[CrossRef](#)]
12. Solberg, S.; Weydahl, D.J.; Astrup, R. Temporal stability of X-band single-pass insar heights in a spruce forest: Effects of acquisition properties and season. *IEEE Trans. Geosci. Remote Sens.* **2015**, *53*, 1607–1614. [[CrossRef](#)]
13. Praks, J.; Demirpolat, C.; Antropov, O.; Hallikainen, M. On forest height retrieval from spaceborne X-band interferometric sar images under variable seasonal conditions. In Proceedings of the XXXII Finnish URSI Convention on Radio Science and SMARAD Seminar, Espoo, Finland, 24–25 April 2013; pp. 115–118.
14. Way, J.; Paris, J.; Kasischke, E.; Slaughter, C.; Viereck, L.; Christensen, N.; Dobson, M.C.; Ulaby, F.; Richards, J.; Milne, A.; et al. The effect of changing environmental-conditions on microwave signatures of forest ecosystems: Preliminary results of the March 1988 Alaskan aircraft sar experiment. *Int. J. Remote Sens.* **1990**, *11*, 1119–1144. [[CrossRef](#)]
15. Solberg, S.; Hansen, E.H.; Gobakken, T.; Naesset, E.; Zahabu, E. Biomass and insar height relationship in a dense tropical forest. *Remote Sens. Environ.* **2017**, *192*, 166–175. [[CrossRef](#)]
16. Solberg, S.; Næsset, E.; Gobakken, T.; Bollandsås, O.-M. Forest biomass change estimated from height change in interferometric sar height models. *Carbon Balance Manag.* **2014**, *9*, 5–17. [[CrossRef](#)] [[PubMed](#)]
17. Solberg, S.; Gizachew, B.; Næsset, E.; Gobakken, T.; Bollandsås, O.M.; Mauya, E.W.; Olsson, H.; Malimbwi, R.; Zahabu, E. Monitoring forest carbon in a tanzanian woodland using interferometric sar: A novel methodology for REDD+. *Carbon Balance Manag.* **2015**, *10*, 14–28. [[CrossRef](#)] [[PubMed](#)]
18. Hoffmann, J.; Walter, D. How complementary are srtm-x and -c band digital elevation models? *Photogram. Eng. Remote Sens.* **2006**, *72*, 261–268. [[CrossRef](#)]
19. Walker, W.S.; Kelldorfer, J.M.; Pierce, L.E. Quality assessment of srtm c- and x-band interferometric data: Implications for the retrieval of vegetation canopy height. *Remote Sens. Environ.* **2007**, *106*, 428–448. [[CrossRef](#)]
20. Neeff, T.; Dutra, L.V.; dos Santos, J.R.; Freitas, C.D.; Araujo, L.S. Tropical forest measurement by interferometric height modeling and p-band radar backscatter. *For. Sci.* **2005**, *51*, 585–594.
21. Gama, F.F.; dos Santos, J.R.; Mura, J.C. Eucalyptus biomass and volume estimation using interferometric and polarimetric sar data. *Remote Sens.* **2010**, *2*, 939–956. [[CrossRef](#)]
22. Mauya, E.W.; Ene, L.T.; Bollandsås, O.M.; Gobakken, T.; Næsset, E.; Malimbwi, R.E.; Zahabu, E. Modelling aboveground forest biomass using airborne laser scanner data in the miombo woodlands of Tanzania. *Carbon Balance Manag.* **2015**, *10*. [[CrossRef](#)] [[PubMed](#)]
23. Ene, L.T.; Næsset, E.; Gobakken, T.; Mauya, E.W.; Bollandsås, O.M.; Gregoire, T.G.; Ståhl, G.; Zahabu, E. Large-scale estimation of aboveground biomass in miombo woodlands using airborne laser scanning and national forest inventory data. *Remote Sens. Environ.* **2016**, *186*, 626–636. [[CrossRef](#)]
24. Ene, L.T.; Næsset, E.; Gobakken, T.; Bollandsås, O.M.; Mauya, E.W.; Zahabu, E. Large-scale estimation of change in aboveground biomass in miombo woodlands using airborne laser scanning and national forest inventory data. *Remote Sens. Environ.* **2017**, *188*, 106–117. [[CrossRef](#)]
25. The United Republic of Tanzania (URT). *National Forestry Resource Monitoring and Assessment of Tanzania (Naforma). Field Manual. Biophysical Survey*; The United Republic of Tanzania: Dar es Salaam, Tanzania, 2010. Available online: <http://www.fao.org/forestry/23484-05b4a32815ecc769685b21b03be44ea77.pdf> (accessed on 10 August 2017).
26. Tomppo, E.; Malimbwi, R.; Katila, M.; Makisara, K.; Henttonen, H.M.; Chamuya, N.; Zahabu, E.; Otieno, J. A sampling design for a large area forest inventory: Case tanzania. *Can. J. For. Res.* **2014**, *44*, 931–948. [[CrossRef](#)]
27. Cochran, W.G. *Sampling Techniques*, 3rd ed.; Wiley: New York, NY, USA, 1977.



28. Tomppo, E.; Katila, M.; Makisara, K.; Malimbwi, R.; Chamuya, N.; Otieno, J.; Dalsgaard, S.; Leppanen, M. A Report to the Food and Agriculture Organization of the United Nations (FAO) in Support of Sampling Study for National Forestry Resources Monitoring and Assessment (NAFORMA) in Tanzania. 2010. Available online: <http://www.suaire.suanet.ac.tz:8080/xmlui/handle/123456789/1296> (accessed on 10 August 2017).
29. Næsset, E.; Ørka, H.O.; Solberg, S.; Bollandsås, O.M.; Hansen, E.H.; Mauya, E.; Zahabu, E.; Malimbwi, R.; Chamuya, N.; Olsson, H.; et al. Mapping and estimating forest area and aboveground biomass in miombo woodlands in tanzania using data from airborne laser scanning, tandem-x, rapideye, and global forest maps: A comparison of estimated precision. *Remote Sens. Environ.* **2016**, *175*, 282–300. [[CrossRef](#)]
30. Tomppo, E.; Gschwantner, T.; Lawrence, M.; McRoberts, R.E. *National Forest Inventories: Pathways for Common Reporting*; Springer Science + Business Media B.V.: Dordrecht, The Netherlands, 2010.
31. Mugasha, W.A.; Eid, T.; Bollandsas, O.M.; Malimbwi, R.E.; Chamshama, S.A.O.; Zahabu, E.; Katani, J.Z. Allometric models for prediction of above- and belowground biomass of trees in the miombo woodlands of tanzania. *For. Ecol. Manag.* **2013**, *310*, 87–101. [[CrossRef](#)]
32. Anon. WorldDEM. Airbus Defense and Space. Available online: <http://www.astrium-geo.com/worldDEM> (accessed on 10 August 2017).
33. Krieger, G.; Moreira, A.; Fiedler, H.; Hajnsek, I.; Werner, M.; Younis, M.; Zink, M. Tandem-x: A satellite formation for high-resolution sar interferometry. *IEEE Trans. Geosci. Remote Sens.* **2007**, *45*, 3317–3341. [[CrossRef](#)]
34. Hansen, M.C.; Potapov, P.V.; Moore, R.; Hancher, M.; Turubanova, S.A.; Tyukavina, A.; Thau, D.; Stehman, S.V.; Goetz, S.J.; Loveland, T.R.; et al. High-resolution global maps of 21st-century forest cover change. *Science* **2013**, *342*, 850–853. [[CrossRef](#)] [[PubMed](#)]
35. Shimada, M.; Itoh, T.; Motooka, T.; Watanabe, M.; Shiraishi, T.; Thapa, R.; Lucas, R. New global forest/non-forest maps from alos palsar data (2007–2010). *Remote Sens. Environ.* **2014**, *155*, 13–31. [[CrossRef](#)]



© 2017 by the authors. Licensee MDPI, Basel, Switzerland. This article is an open access article distributed under the terms and conditions of the Creative Commons Attribution (CC BY) license (<http://creativecommons.org/licenses/by/4.0/>).